JACS
JOURNAL OF THE AMERICAN CHEMICAL SOCIETY
Article
pubs.acs.org/JACS

Direct Copper(III) Formation from O_2 and Copper(I) with Histamine Ligation

J. Brannon Gary,[†] Cooper Citek,[†] Timothy A. Brown,[†] Richard N. Zare,[†] Erik C. Wasinger,[‡] and T. Daniel P. Stack*[,†]

[†]Department of Chemistry, Stanford University, Stanford, California 94305, United States
[‡]Department of Chemistry and Biochemistry, California State University, Chico, California 95929, United States

Supporting Information

ABSTRACT: Histamine chelation of copper(I) by a terminal histidine residue in copper hydroxylating enzymes activates dioxygen to form unknown oxidants, generally assumed as copper(II) species. The direct formation of copper(III)-containing products from the oxygenation of histamine-ligated copper(I) complexes is demonstrated here, indicating that copper(III) is a viable oxidation state in such products from both kinetic and thermodynamic perspectives. At low temperatures, both trinuclear $Cu(II)_2Cu(III)O_2$ and dinuclear $Cu(III)_2O_2$ predominate, with the distribution dependent on the histamine ligand structure and oxygenation conditions. Kinetics studies suggest the bifurcation point to these two products is an unobserved peroxide-level dimer intermediate. The hydrogen atom reactivity difference between the trinuclear and binuclear complexes at parity of histamine ligand is striking. This behavior is best attributed to the accessibility of the bridging oxide ligands to exogenous substrates rather than a difference in oxidizing abilities of the clusters.

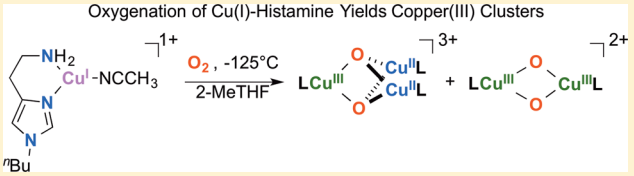

1. INTRODUCTION

Copper enzymes in biology are capable of dioxygen activation at mono-, bi-, and trimetallic active sites.[1] Given this diversity, defining the structure−reactivity relationships between $Cu-O_2$ species is foundational to the understanding of critical redox transformations central to aerobic life. Synthetic systems that faithfully reproduce biological copper(I) ligation and oxygenate to discrete, characterizable species provide chemical precedents for potential reactivity operative in biological systems. While nature typically uses imidazole ligation via the histidine amino acid,[1] synthetic systems are dominated by pyridine, pyrazole, and alkylated amine ligation.[2,3] Several studies of the direct oxygenation of copper(I) imidazole-ligated complexes suggest that μ-η^2:η^2-peroxodicopper(II) ^{S}**P** and *trans*-1,2-peroxodicopper(II) ^{T}**P** species are stabilized by imidazole subunits (Figure 1).[4−9] By comparison, direct oxygenation of copper(I) complexes with imidazole ligation to bis(μ-oxide)-dicopper(III) **O** species or the more elusive trinuclear bis(μ_3-oxide)$Cu(II)_2Cu(III)$ **T** species is heretofore unknown, raising the question of whether imidazole ligation is compatible with direct oxygenation to a copper(III) oxidation state.

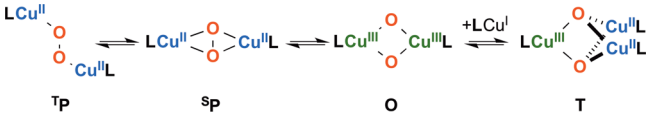

Figure 1. Characterized synthetic dimeric and trimeric copper complexes derived from oxygenation of Cu(I) complexes.

Terminal histamine ligation (a "histidine brace") in copper enzymes is an emerging theme.[1,10−16] It has been most recently characterized in mononuclear polysaccharide monooxygenases, capable of oxidative degradation of cellulose.[10,11] Similar terminal histamine ligation exists in the proposed dicopper active sites of particulate methane monooxygenases (pMMO), which convert methane to methanol,[12−14] and, by structural homology, ammonia monooxygenases (AMO), which convert ammonia to hydroxylamine.[15,16] As this last reaction is essential in the global nitrogen cycle, it is performed on a massive scale on this planet by bacteria and archaea with the associated consumption of dioxygen.[17−19]

While the histamine brace ligation motif has been established in biological systems, the nature of solution reactivity by histamine-ligated copper(I) complexes with dioxygen is unknown. Two ligands containing primary amine substituents have been reported that allow for transiently observed copper-dioxygen adducts by direct oxygenation using stopped-flow experiments, although their stability has restricted characterization.[20,21] Given these current limitations, synthetic model systems that use primary amine ligation in direct oxygenation reactions could inform on this new and unique ligation environment to add insight into its possible use and function in biology.

To alleviate problematic issues of a direct oxygenation with primary amine ligation to Cu(I) complexes, our group recently reported a ligand substitution strategy on a preformed copper-

Received: May 30, 2016
Published: July 28, 2016

DOI: 10.1021/jacs.6b05538
J. Am. Chem. Soc. 2016, 138, 9986−9995

dioxygen species (i.e., core capture).[22,23] Thus, histamine and simple primary amine ligation of dimeric Cu(III) **O** species are accessible indirectly from more easily oxygenated Cu(I) complexes. Herein, we expand on the species formed by *direct* oxygenation of copper(I) histamine-ligated complexes that yield both dimeric **O** and trimeric **T** species (Figure 1). These results mark the first example of imidazole copper(I) ligation that are kinetically and thermodynamically competent to oxygenate directly to form copper(III) species, highlighting that, from a chemical perspective, there is no reason to exclude copper(III) in binuclear or trinuclear copper sites in biological systems that activate dioxygen.

2. RESULTS

2.1. Histamine Ligands. The role of histamine ligation in copper-dioxygen chemistry is expanding due to the recent observations of the histamine brace ligation in copper-dioxygen-dependent enzymes. While this motif is observed in resting forms of the enzymes, the nature of the oxygenated intermediates is unknown experimentally. Oxygenation of synthetic histamine-ligated copper(I) complexes with O_2 to known intermediates is also unrealized. To address this issue, a series of substituted histamine ligands were synthesized (Scheme 1).

Scheme 1. Synthesis of Alkylated Histamine Derivatives[a]

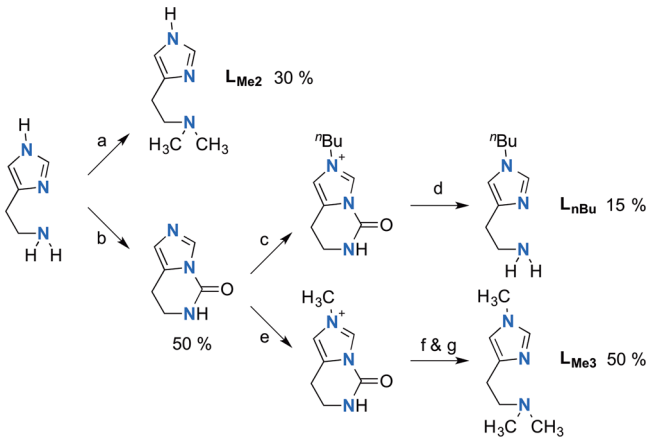

[a]Reaction conditions: (a) paraformaldehyde, $NaBH_3CN$; (b) carbonyldiimidazole; (c) *n*-butyl iodide; (d) 12 M HCl; (e) MeI; (f) 12 M HCl; (g) paraformaldehyde, $NaBH_3CN$.

Eschweiler–Clarke methylation of the amine of histamine is ineffective in producing $\mathbf{L_{Me2}}$, but reductive amination with paraformaldehyde and cyanoborohydride results in an efficient, direct synthesis of the tertiary-amine histamine analogue on gram scale. This amount allows distillation of ligand from calcium hydride, which assures maximal formation of the copper oxygenated intermediates. Methylation of $\mathbf{L_{Me2}}$ to $\mathbf{L_{Me3}}$ using standard methylating agents, however, results in difficult-to-separate mixtures of the N_τ- versus N_π-methyl-imidazoles. An alternative synthetic route to pure $\mathbf{L_{Me3}}$ initially protects the N_π-imidazole position as a cyclic urea, followed by N_τ-alkylation, deprotection, and a reductive amination with paraformaldehyde and cyanoborohydride. Though longer, each step is efficient and reproducible, yielding gram quantities of $\mathbf{L_{Me3}}$. Additionally, functionalization of the cyclic urea intermediate with other alkyl substituents is possible, which proved critical for the subsequent purification of $\mathbf{L_{nBu}}$ through an organic extractive procedure. These modifications allow for study of primary and tertiary amine analogues of histamines along with variable imidazole alkylation, all key properties associated with the biological histamine brace.[1,10−16]

2.2. Direct Oxygenation of Histamine Copper(I) Complexes. Injection of a 1:1 molar solution of $\mathbf{L_{Me3}}$ and copper(I) into an O_2-saturated 2-methyltetrahydrofuran (2-MeTHF) solution at −125 °C yields a distinct but new optical spectrum after 5 min (Figure 2), suggestive of the formation of

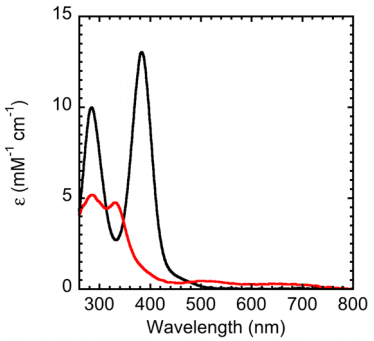

Figure 2. Optical absorption spectra of $\mathbf{O_{Me3}}$ (core capture-black) and the new species (direct oxygenation-red). For comparative purposes, the extinction coefficients are based upon the initial Cu concentration (0.9 mM Cu, 2MeTHF, 1 mm path length, SbF_6^- counterion, −125 °C).

a new copper-dioxygen species. By contrast, the formation of a histamine-ligated dimeric copper(III)-bis-oxide species is possible using a core capture strategy (i.e., ligand substitution) at −125 °C; addition of 2 equiv of $\mathbf{L_{Me3}}$ to the preformed binuclear copper(III) bis-oxide $\mathbf{O_{TMPD}}$ precursor (Scheme 2 and Figure 2) efficiently yields an $\mathbf{O_{Me3}}$ species, previously characterized.[19]

Scheme 2. Core Capture vs Direct Oxygenation with LMe_3 Histamine Ligation

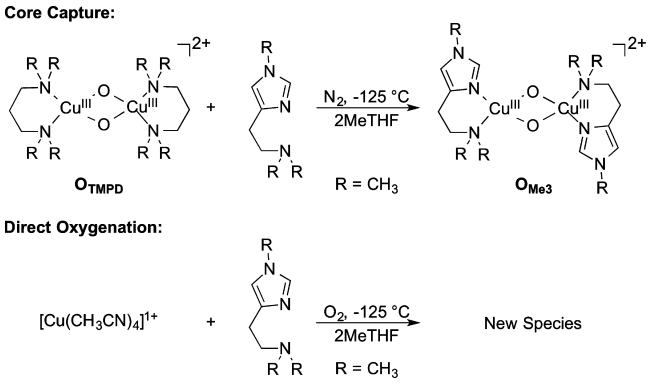

With access to the family of histamine derivatives ($\mathbf{L_{Me3}}$, $\mathbf{L_{nBu}}$, and $\mathbf{L_{Me2}}$), the generalization of the direct oxygenation of copper(I) with histamine ligation was optimized. Addition of 1:1 histamine ($\mathbf{L_{Me3}}$, $\mathbf{L_{nBu}}$, and $\mathbf{L_{Me2}}$) to copper(I) mixtures to an O_2-saturated 2-MeTHF solution at −95 °C yielded, within 3 min, similar spectra for all three histamine derivatives (Scheme 3). $\mathbf{L_{Me2}}$ results in lower intensity absorption features, presumably a result of the lower solubility observed for this ligand and copper mixture. All of these optical spectra are again

DOI: 10.1021/jacs.6b05538
J. Am. Chem. Soc. 2016, 138, 9986−9995

Scheme 3. Trinuclear Complex Formation

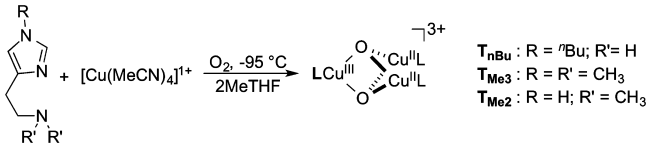

distinctly different from those of their corresponding bis-oxide dimeric **O** species previously synthesized by core capture.[19]

The **O** species formed through core capture (e.g., $\mathbf{O}_{\mathbf{Me3}}$) and the new products of direct oxygenation show markedly different thermal stabilities. For example, using the $\mathbf{L}_{\mathbf{Me3}}$ ligand creates a new species that is stable at −80 °C with a half-life ($t_{1/2}$) of ca. 6 min at −40 °C. By comparison, dimeric $\mathbf{O}_{\mathbf{Me3}}$ is less thermally stable, with a $t_{1/2}$ of 50 min at −80 °C. The thermal stability difference is even more striking with the primary amine containing *n*-butyl histamine ligand ($\mathbf{L}_{\mathbf{nBu}}$); the direct oxygenation product is stable at −80 °C, but decays with a $t_{1/2}$ of 60 min at −40 °C. This relatively high thermal stability is not observed with the comparable bis-oxide $\mathbf{O}_{\mathbf{nBu}}$ that thermally decomposes quickly at −80 °C ($t_{1/2}$ = 1 min). Thus, the distinctly different optical absorption spectra and thermal stabilities indicate that core capture and direct oxygenation produce distinctly different but low-temperature stable copper-dioxygen species.

2.3. Trinuclear Cluster Characterization. *2.3.1. O_2 Uptake Experiments.* In an effort to establish the Cu-to-O_2 ratio in the direct oxygenation of copper(I) with histamine ligation, the product formation was monitored as a function of substoichiometric equivalents of O_2. Using a 10 mM [Cu(I)$\mathbf{L}_{\mathbf{nBu}}$]$SbF_6$ solution in 2-MeTHF, dioxygen-saturated tetrahydrofuran (10 mM)[24] was added in 0.1 equiv aliquots, and the cluster formation was monitored optically. Maximal cluster formation for the new species using $\mathbf{L}_{\mathbf{nBu}}$ was observed at 0.33 equiv of O_2 or a Cu-to-O_2 ratio of 3.0:1.0. The simplest interpretation of this stoichiometry is that the direct oxygenation product is a trinuclear copper cluster.[25−29] Analogous O_2 titrations with 10 mM [Cu(I)$\mathbf{L}_{\mathbf{Me3}}$]$SbF_6$ solutions in 2-MeTHF yielded maximal absorbances with 0.31 equiv of O_2 or a Cu to O_2 ratio of 3.2:1.0, again consistent with characterization of a trinuclear copper cluster.[25−29] The direct oxygenated products with $\mathbf{L}_{\mathbf{nBu}}$, $\mathbf{L}_{\mathbf{Me3}}$, and $\mathbf{L}_{\mathbf{Me2}}$ will be designated as $\mathbf{T}_{\mathbf{nBu}}$, $\mathbf{T}_{\mathbf{Me3}}$, and $\mathbf{T}_{\mathbf{Me2}}$, respectively.

2.3.2. UV−Vis Spectroscopy. The resulting optical spectra of the newly formed species (Figure 3) are similar to the optical spectra observed for other bis-oxide trinuclear species, **T**, one example of which has been characterized structurally with a localized valence Cu(III)Cu(II)Cu(II) core (Figure 1).[25] All previously observed **T** species exhibit two intense UV and two lower-intensity visible features.[25−29] Consistent with other reported systems, $\mathbf{T}_{\mathbf{nBu}}$, $\mathbf{T}_{\mathbf{Me3}}$, and $\mathbf{T}_{\mathbf{Me2}}$ exhibit at least two intense UV and two lower-intensity visible features (Figure 3),[25−29] although blue-shifted compared to other reported complexes (Table 1). Specifically, optical transitions of $\mathbf{T}_{\mathbf{Me3}}$ and $\mathbf{T}_{\mathbf{Me2}}$ are on the high-energy side of reported **T** species. In fact, only the anionically ligating *β*-diketiminate ligand disclosed by Gupta et al. has a more blue-shifted absorption spectrum.[28] With the significant blue-shifting of $\mathbf{T}_{\mathbf{nBu}}$, an additional much less intense visible feature is also observed at 686 nm.

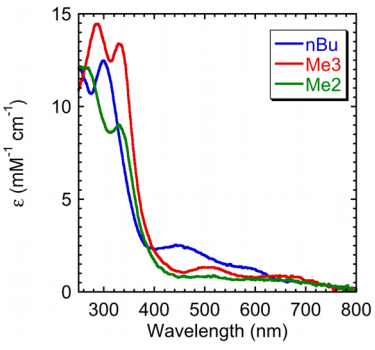

Figure 3. Observed optical absorption spectra of direct oxygenation products of the Cu(I) complexes of $\mathbf{L}_{\mathbf{nBu}}$ (blue), $\mathbf{L}_{\mathbf{Me3}}$ (red), and $\mathbf{L}_{\mathbf{Me2}}$ (green) assuming a trinuclear copper composition (0.9 mM Cu, 2MeTHF, 1 mm path length, SbF_6^- counterion, −95 °C).

2.3.3. Dinuclear O to Trinuclear T Cluster Conversion. Further evidence of the **T** cluster formation during direct oxygenation results from the addition of 1 equiv of [Cu(I)$\mathbf{L}_{\mathbf{Me3}}$]$SbF_6$ to a deoxygenated solution of $\mathbf{O}_{\mathbf{Me3}}$, formed by core capture at −125 °C (Scheme 4). This sequence cleanly converts the $\mathbf{O}_{\mathbf{Me3}}$ optical spectrum to that of $\mathbf{T}_{\mathbf{Me3}}$ in 30 min (Figure 4). This conversion corroborates the simplest assignment of $\mathbf{T}_{\mathbf{Me3}}$ as a cluster with three copper centers.

The slow rate of this conversion is striking given that the direct oxygenation of [Cu(I)$\mathbf{L}_{\mathbf{Me3}}$]$SbF_6$ at −125 °C is complete in 5 min. Addition of 1 equiv of [Cu(I)$\mathbf{L}_{\mathbf{Me3}}$]$CF_3SO_3$ to $\mathbf{O}_{\mathbf{Me3}}$-$SbF_6$ accelerates the rate of conversion 3-fold (10 min). With exclusive use of $CF_3SO_3^-$ anions for both reactants, the conversion is accelerated 30-fold (1 min) (Table 2).

2.3.4. Cu K-Edge X-ray Absorption Spectroscopy (XAS). The only crystallographically characterized **T** cluster, reported nearly 20 years ago, shows a valence-localized Cu(III)Cu(II)-Cu(II) formulation with C_2 symmetry, with 2.64 Å Cu(II)−Cu(II) and 2.70 Å Cu(III)−Cu(II) distances, along with short Cu(III)−O distances at 1.84 Å.[25] The Cu K-edge EXAFS model of $\mathbf{T}_{\mathbf{Me3}}$ (Figure 5) requires each copper to have two copper scatterers at an averaged distance of 2.67 Å, consistent with a DFT-optimized structure ($Cu-Cu_{average}$ 2.67 Å − vide infra) and the previous crystal structure.[25] EXAFS resolution does not allow separation of the Cu−Cu distances, though the coordinating ligand shells can be separated into one short Cu−N/O shell at 1.92 Å and three Cu−N/O scatters at 2.03 Å. The Cu K-edge pre-edge is dominated by the Cu(II) feature at 8979 eV, obscuring the less intense Cu(III) feature typically found near 8981 eV.[30,31]

2.3.5. High-Resolution Mass Spectrometry. In an effort to further characterize the cluster composition, high-resolution mass spectrometry was used to establish the atomic composition of the copper clusters. Using this technique, $\mathbf{T}_{\mathbf{nBu}}$ is observed as a monocation with two SbF_6^- anions at *m*/*z* of 1195.99001 (theoretical 1195.99189) with a distinct isotope pattern, which is characteristic of three copper and two antimony atoms (Figure 6). $\mathbf{T}_{\mathbf{Me3}}$ is also observed as a monocation with two SbF_6^- anions at *m*/*z* of 1153.94277 (theoretical 1153.94494) and matching isotope pattern.

2.3.6. Trinuclear Cluster Formation Yields. The formation of a trinuclear cluster produces a distinct optical spectrum from other copper-dioxygen-derived thermally sensitive intermediates. The molar extinction coefficients of $\mathbf{T}_{\mathbf{nBu}}$, $\mathbf{T}_{\mathbf{Me3}}$, and $\mathbf{T}_{\mathbf{Me2}}$ are in line with other reported trinuclear clusters (Table 1) but do not establish a yield for their formation. $\mathbf{T}_{\mathbf{nBu}}$, $\mathbf{T}_{\mathbf{Me3}}$, and $\mathbf{T}_{\mathbf{Me2}}$ react rapidly with decamethylferrocene (Scheme 5), providing a convenient titration method to assess their formation yields by following the disappearance of their

DOI: 10.1021/jacs.6b05538
J. Am. Chem. Soc. 2016, 138, 9986−9995

Table 1. Optical Features of Trinuclear Clusters T_{nBu}, T_{Me3}, T_{Me2}, and Literature Trinuclear Clusters

	λ_{max} (nm) and ε (mM^{-1} cm^{-1})					
optical transition	T_{nBu}	T_{Me3}	T_{Me2}	T[a]	T[b]	T[c]
1	250 (12.1)	285 (14.7)	264 (12.0)	290 (12.6)	N/A	N/A
2	300 (12.6)	332 (13.5)	330 (9.0)	355 (15.0)	345 (12.6)	342 (12.0)
3	443 (2.5)	507 (1.4)	505 (0.9)	480 (1.4)	500 (1.3)	515 (1.0)
4	580 (1.3)	655 (0.9)	658 (0.6)	620 (0.8)	620 (0.9)	685 (0.8)

[a] *N,N,N′,N′*-(*R,R*)-1,2-Cyclohexanediamine.[25] [b] *N,N,N′,N′*-Tetramethylethylenediamine.[27] [c] *N,N*-Dimethyl-2-(2-pyridyl)ethylamine.[26]

Scheme 4. O-to-T Cluster Conversion

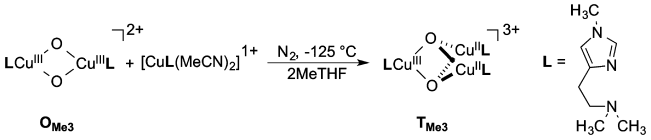

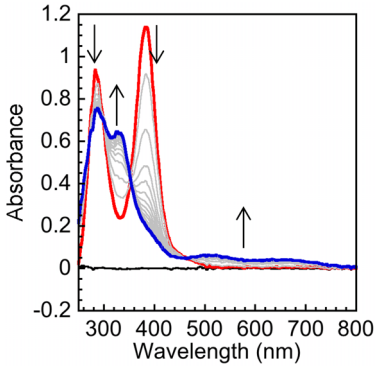

Figure 4. Optical absorption time trace of O_{Me3} (red) converting to T_{Me3} (blue) by the addition of 1 equiv of [Cu(I)L_{Me3}]SbF_6 (1.5 mM total Cu, 2MeTHF, 1 mm path length, −125 °C).

Table 2. Addition of Cu(I) to Preformed O_{Me3} Species

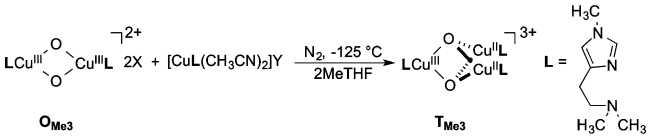

X^-	Y^-	formation time (min)
SbF_6^-	SbF_6^-	30
SbF_6^-	$CF_3SO_3^-$	10
$CF_3SO_3^-$	$CF_3SO_3^-$	1

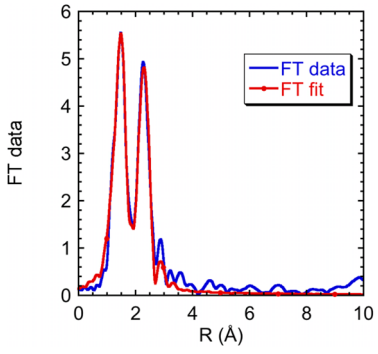

Figure 5. Fourier transform fit of the T_{Me3} EXAFS data.

characteristic UV and visible absorption features (see Supporting Information). Assuming the Cu_3O_2 core as a one-electron oxidant, the titration of T_{nBu} suggests greater than 70% formation. A similar optical titration of the permethylated analogue T_{Me3} quantifies its formation at 80% and the N−H imidazole derivative (T_{Me2}) at 40%. The presence of the amine N−H groups impacts not only the formation yield but also the thermal stability of the trinuclear cluster (vide supra).

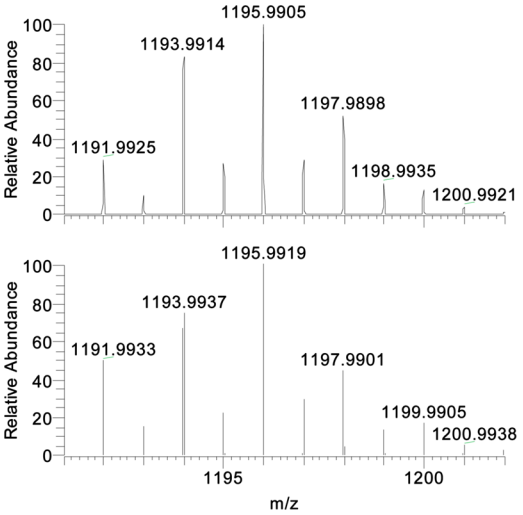

Figure 6. Electrospray high-resolution mass spectra of T_{nBu}: top, experimentally observed isotope pattern; bottom, theoretical predicted isotope pattern for $[(L_{nBu}Cu)_3O_2(SbF_6)_2]^+$.

Scheme 5. Trinuclear Cluster Formation Yields by Redox Titrations

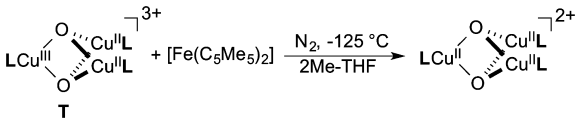

2.4. Modified Reaction Conditions: Temperature and Concentration. In the standard formation conditions described above, the total copper concentration is ca. 1 mM, and the reaction temperature is −95 °C. Under these conditions, only the trinuclear clusters T_{nBu} and T_{Me3} are discernible products from the optical spectra in the direct oxygenation reactions. In an effort to modulate cluster formation, temperature and concentration were adjusted to ascertain their effect on cluster formation. Oxygenation of 1 mM [Cu(I)L_{nBu}]SbF_6 at −125 °C results in a more complex optical spectrum, which is resolvable to a 5:1 ratio of the T_{nBu} and O_{nBu} species (Scheme 6); this analysis is possible using the known optical spectra of T_{nBu} and O_{nBu} species, which each possess characteristically intense ligand-to-metal charge transfer (LMCT) optical bands.[22] By contrast, 1 mM [Cu(I)L_{Me3}]SbF_6 cleanly oxygenates to T_{Me3} at −125 °C. Lowering the concentration of [Cu(I)L_{Me3}]SbF_6 to 0.1 mM, however, yields

DOI: 10.1021/jacs.6b05538
J. Am. Chem. Soc. 2016, 138, 9986−9995

Scheme 6. Trinuclear/Binuclear Mixture Formation

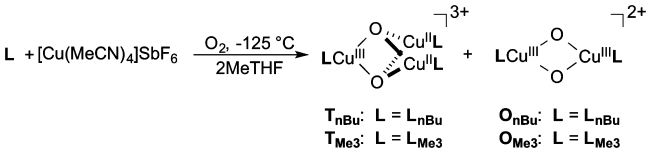

a spectrum resolvable to a 3.5:1 mixture of trinuclear $\mathbf{T_{Me3}}$ and dimeric $\mathbf{O_{Me3}}$. These results indicate that concentration, temperature, and ligand steric demands impact the product distribution of the direct oxygenation reaction; ligands with lesser steric demands require colder temperatures and lower copper concentrations to form any appreciable **O** species. These results provide possible insights into cluster formation mechanisms operative during direct oxygenation conditions (vide infra).

2.5. Comparative Cluster Reactivity with Exogenous Substates. With access to both **O** and **T** species at parity of histamine ligation, reactivity comparison with a hydrogen atom donor substrate could be investigated (Scheme 7). $\mathbf{T_{Me3}}$ (0.33

Scheme 7. Trinuclear/Binuclear Relative Proton-Coupled Electron-Transfer Reactivity

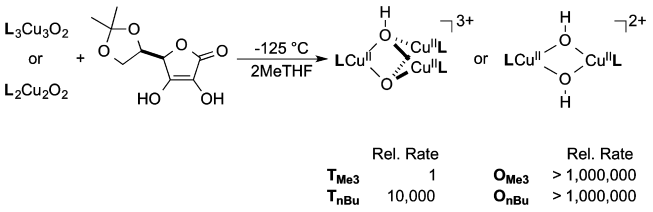

mM) undergoes first-order decay with 50 equiv of 5,6-isopropylidene ascorbic acid with a k_{obs} of 0.02 min^{-1}; the rate of reaction with $\mathbf{O_{Me3}}$ is estimated to be at least 10^6 faster. The latter estimate required using 10-fold less of the ascorbic acid substrate and more dilute reaction conditions.[32] The dramatic reaction rate difference between clusters is confirmed in the competitive experiment of adding substoichiometric amounts of ascorbic acid to $\mathbf{O_{Me3}}/\mathbf{T_{Me3}}$ mixtures; at −125 °C only selective reduction of the optical features of the $\mathbf{O_{Me3}}$ species is observed. After selective $\mathbf{O_{Me3}}$ reduction, $\mathbf{O_{Me3}}/\mathbf{T_{Me3}}$ ratios are unchanged with time, indicating no appreciable interconversion of **O** and **T** clusters. A similar reactivity behavior is observed for $\mathbf{O_{nBu}}/\mathbf{T_{nBu}}$ mixtures, except that the difference in their reaction rates is measured to be only 100-fold. The faster absolute rates of $\mathbf{O_{nBu}}$ and $\mathbf{T_{nBu}}$ species limits the ability to differentiate these complexes.[32] Trinuclear species react with substrates at significantly slower rates than their related binuclear species.

The comparison of the reaction rates between related species, differentially ligated, is also interesting at −125 °C. $\mathbf{T_{nBu}}$, a less sterically encumbered species compared to $\mathbf{T_{Me3}}$, reacts 10 000 times faster with 5,6-isopropylidene ascorbic acid. By contrast, access to the dimeric cores is similar, as $\mathbf{O_{nBu}}$ reacts only 10-fold faster than $\mathbf{O_{Me3}}$.[22]

In an attempt to understand the relative substrate reactivity of the **O** and **T** clusters, a series of isodesmic reactions for comparison of electron and H-atom affinities were examined computationally (Scheme 8). Optimizations of all clusters used a M06 functional, tzvp basis set, and an SMD solvation model,[33−37] followed by a second-order relativistic corrected

Scheme 8. Isodesmic Comparisons of Trinuclear and Binuclear Clusters for Electron and H-Atom Transfers

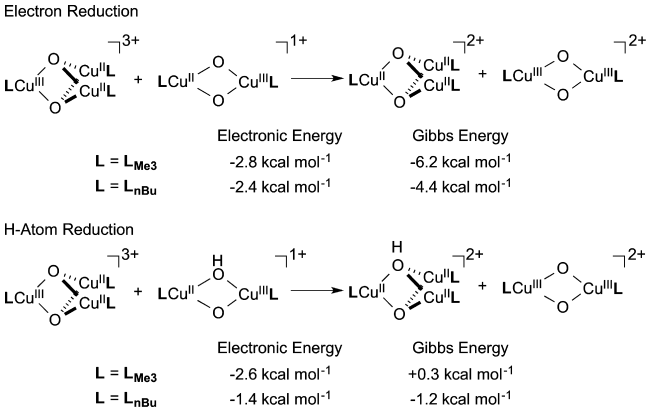

(DKH2) single-point energy,[37] a methodology that successfully correlates and theoretical free energies of Cu(II) and Cu(III) species.[19] The optimization of $\mathbf{T_{nBu}}$ as a triplet reproduces the valence-localized Cu(III)Cu(II)Cu(II) electronic structure, consistent with previous calculations, and the previously structurally characterized trinuclear cluster.[25,38−40] The relative positioning of the histamine ligands on the **T** cluster generates several isomers (Figure 7), the most stable of which positions

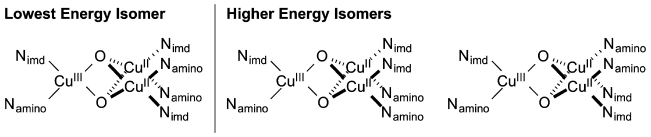

Figure 7. Possible histamine isomers in trinuclear complexes.

the two Cu(II) ligands in a *trans* orientation; this isomer is 3−5 kcal mol^{-1} more stable. The lowest energy one-electron and H-atom reduced species are calculated to be pseudo-C_3 symmetric quartet species with a Cu(II)Cu(II)Cu(II) electronic structure. The *trans* arrangement of the histamine ligands in the **O** species is also preferred energetically, although the energy difference is small (<1 kcal mol^{-1}). Both the one-electron and H-atom reduced species are calculated to be valence-localized doublet species.

The isodesmic reaction of the reduced, mixed-valent $\mathbf{O_{Me3}}$ species with the $\mathbf{T_{Me3}}$ species is predicted to have a favorable free energy of −6.2 kcal mol^{-1} evaluated at 298 °C, suggesting that the $\mathbf{T_{Me3}}$ species is a more powerful oxidant. Comparing the electron reduction affinity between $\mathbf{O_{nBu}}$ and $\mathbf{T_{nBu}}$, the reduced $\mathbf{T_{nBu}}$ is favored by ca. 4 kcal mol^{-1}. The favorable predicted formation of $\mathbf{T_{Me3}}$ and $\mathbf{T_{nBu}}$ indicate that these clusters are 200−300 mV stronger one-electron oxidants than their binuclear analogues. Comparison of the H-atom affinity of the binuclear **O** versus trinuclear **T** species through isodesmic reactions is also illustrated in Scheme 8. The H-atom reduced **T** clusters are effectively isoenergetic with their **O** analogues, suggesting comparable H-atom affinities.

It is difficult to decouple the inherent reactivity of the **O** and **T** species from effects attributable to steric demands. In an effort to deconvolute the steric and electronic components controlling reduction of **O** and **T** species, the Marcus self-exchange reorganizational energy (λ) values of $\mathbf{T_{Me3}}$, $\mathbf{T_{nBu}}$, $\mathbf{O_{Me3}}$, and $\mathbf{O_{nBu}}$ were estimated from their difference between the electronic ground state and the excited state. The electronic

DOI: 10.1021/jacs.6b05538
J. Am. Chem. Soc. 2016, 138, 9986−9995

ground-state energy is estimated as the sum of the cluster and its one-electron reduced optimized forms, while the excited state energy is estimated from two single-point calculations in which ground-state optimized geometries have exchanged electronic configurations. One-quarter of this reorganization energy ($\lambda/4$) approximates the electronic component or intrinsic barrier of the one-electron or H-atom reduction of the copper clusters.[41]

The calculated self-exchange energy for one-electron reduction for all four species is ca. 20 kcal mol^{-1} and differs by less than 1.7 kcal mol^{-1} between all four self-exchange reactions (Table 3). The estimated reaction barriers are small,

Table 3. Estimated Self-Exchange Reorganizational Energies for Electron and H-Atom Transfers by DFT[a]

	electron transfer		H-atom transfer	
	λ	$\lambda/4$	λ	$\lambda/4$
$\mathbf{T}_{\mathbf{nBu}}$	19.0	4.8	23.1	5.8
$\mathbf{O}_{\mathbf{nBu}}$	19.4	4.8	24.5	6.1
$\mathbf{T}_{\mathbf{Me3}}$	20.7	5.2	24.8	6.2
$\mathbf{O}_{\mathbf{Me3}}$	19.5	4.9	25.3	6.3

[a]Energies are given in kcal mol^{-1}. *n*-Butyl groups of $\mathbf{T}_{\mathbf{nBu}}$ and $\mathbf{O}_{\mathbf{nBu}}$ are modeled as methyl groups.

at ca. 5 kcal mol^{-1}, with a variation of only 0.4 kcal mol^{-1}. Although slightly higher, the calculated self-exchange energy for reduction by an H-atom for all four species is ca. 24 kcal mol^{-1}, which translates to a reaction barrier of 5.8−6.3 kcal mol^{-1} (Table 3). Assuming similar solvation reorganizational energies for both **T** and **O** clusters, the electronic component to the barrier of reduction appears to be a minor contributor and cannot account for the 10^4−10^6 rate differences experimentally observed.

Space-filling models of the four clusters studied for reactivity ($\mathbf{T}_{\mathbf{Me3}}$, $\mathbf{T}_{\mathbf{nBu}}$, $\mathbf{O}_{\mathbf{Me3}}$, and $\mathbf{O}_{\mathbf{nBu}}$) with a *trans* disposition of ligands provide a clear perspective of the access to the copper-oxide cores of each cluster (Figure 8). Histamine methylation in $\mathbf{T}_{\mathbf{Me3}}$ clearly imparts significant steric protection of the oxide ligands

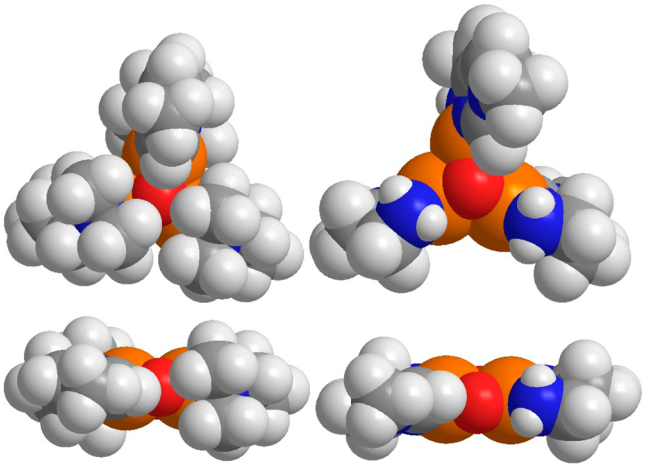

Figure 8. Space-filling models for the calculated structures *trans*-$\mathbf{T}_{\mathbf{Me3}}$ (top left), *trans*-$\mathbf{T}_{\mathbf{nBu}}$ (top right), *trans*-$\mathbf{O}_{\mathbf{Me3}}$ (bottom left), and *trans*-$\mathbf{O}_{\mathbf{nBu}}$ (bottom right). The *n*-butyl groups of $\mathbf{T}_{\mathbf{nBu}}$ and $\mathbf{O}_{\mathbf{nBu}}$ are modeled and illustrated as methyl groups. Color code: orange = copper; red = oxygen; blue = nitrogen; gray = carbon; white = hydrogen.

in both **T** and **O** clusters from external substrates. Previous calculations by our group suggest that linear attack of a C−H bond along the O−O bond vector of the **O** species is the lowest energy pathway to C−H activation, presumably the same mechanism of attack operative in the **T** clusters.[22]

3. DISCUSSION

The role of the copper(III) oxidation state in biology has been discounted generally because of the lack of known ligands present in biology that can stabilize a synthetic copper(III) containing cluster or spectroscopic observation of copper(III) in biological systems. The very positive reduction potentials for mononuclear copper(III) centers ligated by biologically relevant ligands generally argue against its role in biology.[42,43] This work provides a new perspective given the propensity for histamine-ligated copper(I) species to react with dioxygen to form copper(III)-containing trinuclear **T** clusters and, under specialized conditions, copper(III)-containing **O** species with biological histamine ligation. This result highlights that imidazole ligation is viable to facilitate the formation of high-valent copper(III) species. Remarkably, this system tolerates the generally oxidatively susceptible primary amine ligation of $\mathbf{L}_{\mathbf{nBu}}$, which, to our knowledge, is the first example of the direct oxygenation to a stable and characterizable copper-dioxygen adduct. Previous reports by Schindler have illustrated that tetradentate ligation containing primary amines are viable to form superoxide or $^{\mathrm{T}}\mathbf{P}$ species transiently, observable by stop flow methods, but these species have not been further characterized.[20,21] By adjusting the concentration and temperature, synthetic histamine-ligated copper(I) species are competent kinetically to oxygenate directly to dimeric $\mathbf{O}_{\mathbf{nBu}}$ or $\mathbf{O}_{\mathbf{Me3}}$ species with potential relevance to the binuclear active-site oxidants of pMMO and AMO.[22] In this study, the formation of $\mathbf{O}_{\mathbf{nBu}}$ or $\mathbf{O}_{\mathbf{Me3}}$ is complicated by the thermodynamic preference for trinuclear formation, a complication not encountered in pMMO or AMO due to the site-isolation of their dimeric copper active sites.

In general, the trinuclear cluster has been a minority species in copper-dioxygen chemistry due to the dearth of ligand systems that are known to form and stabilize these very compact cores; ligands with minimal steric demands are required.[25−29,38−40] The comparatively low intensity and highly blue-shifted nature of the **T** absorption features, as compared to **O**, $^{\mathrm{S}}\mathbf{P}$, and $^{\mathrm{T}}\mathbf{P}$, make it easy to discount **T** formation for possible indiscriminate copper(II) byproducts when monitoring oxygenation reactions by UV−vis spectroscopy. The optical features for $\mathbf{T}_{\mathbf{nBu}}$, $\mathbf{T}_{\mathbf{Me3}}$, and $\mathbf{T}_{\mathbf{Me2}}$ are significantly blue-shifted from those previously reported, further complicating their characterization.[25−29] This blue-shifting is analogous with our previous reports of **O** species ligated by $\mathbf{L}_{\mathbf{nBu}}$, which acts as a more strongly donating ligand, presumably raising the energy of the accepting orbitals for the LMCT bands.[22,23] Consistent with these observations, the primary amine of $\mathbf{L}_{\mathbf{nBu}}$ is the most blue-shifted of all **T** clusters known. Using a combination of UV−vis, XAS, mass spectrometry, and O_2 stoichiometry, the formation of copper(III)-containing trinuclear **T** clusters by direct oxygenation is shown to be viable.

With the few ligands known to produce **T** clusters, the mechanism of **T** cluster formation has remained elusive. Fukuzami and Itoh have demonstrated that dimeric **O** species can serve as a precursor on the pathway to **T** cluster formation, although their results do not indicate if the **O** species is the direct precursor to **T** formation or if an unobserved

DOI: 10.1021/jacs.6b05538
J. Am. Chem. Soc. 2016, 138, 9986−9995

intermediate is required for the transformation.[26] In this work, the addition of $[Cu(I)\mathbf{L}_{Me3}]SbF_6$ to preformed $\mathbf{O}_{Me3}$ provides insights into the generic **T** cluster formation mechanism. Specifically, the 30 min reaction time for $\mathbf{O}_{Me3}$-to-$\mathbf{T}_{Me3}$ conversion is striking, given that the direct oxygenation of $[Cu(I)\mathbf{L}_{Me3}]^+$ at −125 °C is complete in 5 min—$\mathbf{O}_{Me3}$ cannot be on the direct $\mathbf{T}_{Me3}$ formation pathway. Though not observed optically (Scheme 9), an intermediate species is required.

Scheme 9. Proposed T Formation Mechanism

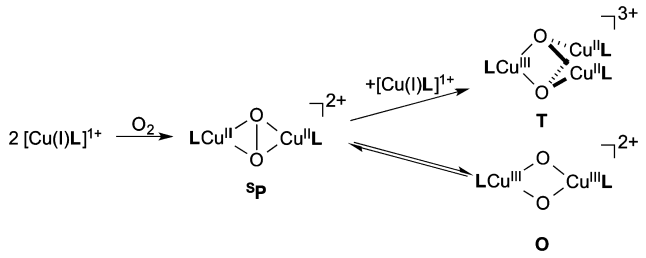

Triflate ($CF_3SO_3^-$) counterions are known to bias $^S\mathbf{P} \rightleftarrows \mathbf{O}$ equilibria toward the $^S\mathbf{P}$ species more than the less coordinating SbF_6^- anion.[44−46] We observe that the addition of triflate anions accelerates the $\mathbf{O}_{Me3}$-to-$\mathbf{T}_{Me3}$ conversion. A mechanistic hypothesis consistent with these observations is that **T** formation proceeds through the addition of a copper(I) species to a peroxide-level intermediate, which we postulate as an $^S\mathbf{P}$ species (Scheme 9).

The **T** species formation mechanism above (Scheme 9) is consistent with the **O** and **T** cluster formations observed experimentally. Cluster selectivity should be tunable, given that the **T** species formation, but not the **O** species formation, is copper(I) concentration dependent. From other studies, **O** species are known to be favored enthalpically relative to their isomeric $^S\mathbf{P}$ forms;[45,47] lower temperature oxygenations should bias $^S\mathbf{P} \rightleftarrows \mathbf{O}$ equilibrium positions toward the **O** species. Consistent with these predictions, lowering the temperature with $[Cu(I)\mathbf{L}_{nBu}]SbF_6$ from −95 to −125 °C results in increased relative formation of $\mathbf{O}_{nBu}$, and lowering the concentration of $[Cu(I)\mathbf{L}_{Me3}]SbF_6$ from 1 to 0.1 mM Cu at −125 °C results in increased formation of $\mathbf{O}_{Me3}$. The temperature and concentration dependence of **T** versus **O** formation is consistent with a bifurcation point to these two products through an unobserved peroxide-level dimer intermediate, postulated as an $^S\mathbf{P}$ species.

It is difficult to decouple the inherent redox reactivity of the **O** and **T** species from effects attributable to steric demands. Isodesmic reactions from DFT calculations predict that, at ligand parity, the trinuclear **T** cluster is a 200−300 mV stronger oxidant than its related binuclear **O** analogue. Similar isodesmic reactions involving a H-atom transfer between **T** and **O** clusters suggest nearly equivalent H-atom affinities. This latter result suggests comparable proton-coupled electron transfer (PCET) reaction rates, which are not consistent with our experiments. The Marcus self-exchange intrinsic barrier differences between $\mathbf{T}_{Me3}$ and $\mathbf{O}_{Me3}$ are ca. 0.5 kcal mol^{-1} for H-atom exchange, while the 10^6 difference in reaction rate with ascorbic acid, a H-atom substrate, would indicate an expected difference of at least 4 kcal mol^{-1} at −125 °C. With the estimated intrinsic barrier representing a small rate differentiation, steric demands are implicated as the main component of the impressive reduction rate difference. We postulate that this dramatic difference results from the accessibility difference of the oxide ligands of the trinuclear core: the less sterically demanding $\mathbf{L}_{nBu}$ permits faster reactivity due to the greater exposure of the oxide ligands and the low barrier pathway for injection of an electron or hydrogen atom into the cluster. This kinetic rate difference highlights the highly compact core present in **T** clusters, necessitating the use of sterically small ligands for its formation in general. The contracted Cu−Cu vectors by ca. 0.1 Å in the **T** cluster compared to the **O** clusters contributes additional steric protection of the oxide ligand in $\mathbf{T}_{Me3}$ and $\mathbf{T}_{nBu}$. Our previous report, with the reactivity of simple diamines in **O** being enhanced by limiting the steric demands of the supporting ligands, is consistent with the observations of steric effects in the reactivity of **T** clusters.[20] Also, selective reactivity of the **O** species in **O**/**T** mixtures highlights that these clusters are not in equilibrium with each other.

4. CONCLUSION

The role of copper(III) in biology is reasonably discounted for mononuclear copper systems due to their very positive reduction potentials with biological ligation.[42,43] However, here faithful biological ligation of copper(I) *directly* yields two different copper(III)-containing clusters with dioxygen. All told, our results indicate that trinuclear copper oxide **T** clusters are the thermodynamically preferred product in a homogeneous solution with sufficiently non-sterically demanding amine or imidazole ligands, although binuclear **O** clusters can also be formed. These **T** species are also more thermally stable and less reactive with substrates than their **O** counterparts. These complexes represent the first example of copper(I) biological ligation (histamine brace) that is kinetically competent to form copper(III) species as the thermodynamic product directly from O_2, hinting at its potential importance in multinuclear copper enzymes in biology.

5. EXPERIMENTAL DETAILS

5.1. General Information. All chemicals were obtained from commercial sources if not mentioned otherwise. THF solvent was of HPLC grade and further purified by a Pure-Solv 400 solvent purification system (Innovative Technology) before storage over molecular sieves. 2-MeTHF (unstabilized, Aldrich) was degassed under vacuum and stored under a N_2 atmosphere, over 3 Å molecular sieves. $[Cu(MeCN)_4]SbF_6$ was synthesized from Cu_2O (Aldrich) and hexafluoroantimonic acid (Aldrich) by a variation of a literature method.[48] Preparation and manipulation of air-sensitive materials were carried out in a N_2 drybox (MBraun). Low-temperature UV−vis spectra were collected on a Varian Cary 50 Scan spectrophotometer with fiber-optic leads to a custom-designed quartz immersion probe (Hellma) of 0.1 or 1 cm optical path length in a custom-designed sample cell (ChemGlass). Reactions at −125 and −95 °C were maintained by $N_2(l)$/pentane and $N_2(l)$/acetone baths, respectively. ^1H NMR spectra were collected in $CDCl_3$ on an Inova 300 MHz, Varian 400 MHz, or Mercury 400 MHz instrument. Reaction kinetics were followed by either single-wavelength (310, 363, or 380 nm) or multi-wavelength (200−1000 nm) monitoring. Kinetic analyses were performed with SPECFIT 3.0.14 program.

All MS data were acquired on an LTQ Orbitrap XL hybrid mass spectrometer (Thermo Fisher Scientific, San Jose, CA, USA). Analyte solutions were drawn and infused by a manual syringe through a commercial source set at position D. The spray potential was held at 3.4 kV, and the sheath gas was set to 100 for 100 psi N_2. The Orbitrap ion-transfer capillary was held at 275 °C. The resolution was set to 60 000 at m/z = 400 for all analyses. All data were analyzed using the Qual Browser feature of the Xcalibur program (Thermo Fisher Scientific).

5.2. Preparation of Materials. Tetramethylpropylene diamine was obtained from Aldrich. Ligands were stirred over CaH_2 under N_2

DOI: 10.1021/jacs.6b05538
J. Am. Chem. Soc. 2016, 138, 9986−9995

atmosphere before vacuum distillation unless stated otherwise. Histamine free base was purchased from Matrix Scientific. 5,6-Isopropylidene-L-ascorbic acid (Aldrich) was dried in a vacuum oven before use. $\mathbf{O}_{\mathbf{nBu}}$ and $\mathbf{O}_{\mathbf{Me3}}$ were prepared according to literature methods.[19]

5.3. Synthesis of N_τ-*n*-Butyl-histamine ($\mathbf{L}_{\mathbf{nBu}}$). N_τ-*n*-Butyl-histamine was synthesized from histamine free base according to the common method of N_τ-alkylation through a cyclic urea intermediate.[49] 7,8-Dihydro-6*H*-imidazo[1,5-*c*]pyrimidin-5-one (2.9 g, 21 mmol, CAS Registry Number 14509-66-1) and iodobutane (4.3 g, 23 mmol) were stirred in 50 mL of DMF at 40 °C overnight. DMF solvent was removed under vacuum. The residue was refluxed in 40 mL of concentrated aqueous HCl overnight. A purple vapor indicating gaseous iodine was observed evolving from the refluxing mixture. The aqueous HCl was removed entirely by rotary evaporation, concurrent with sublimation of additional iodine. Next, 20 mL of 4 M aqueous NaOH was added before extraction three times with 30 mL of dichloromethane. The organic extracts were combined, dried over granular Na_2SO_4, and concentrated. The crude oil was stirred over crushed CaH_2 overnight before heated distillation under vacuum to give a clear viscous oil. Yield: 0.447 g, 13%. ^{1}H NMR (400 MHz, $CDCl_3$): δ 7.31 (s, 1H, aromatic H), δ 6.62 (s, 1H, aromatic H), δ 3.80 (t, 2H, $-CH_2-$), δ 2.92 (t, 2H, $-CH_2-$), δ 2.62 (t, 2H, $-CH_2-$), δ 1.67 (quint., 2H, $-CH_2-$), δ 1.25 (sext., 2H, $-CH_2-$), δ 0.87 (t, 3H, CH3). ^{13}C NMR (100.6 MHz, $CDCl_3$): δ 140.74, δ 136.62, δ 115.79, δ 46.79, δ 42.06, δ 33.13, δ 32.57, δ 19.87, δ 13.64. HRMS (H^+): m/z = 168.1499 ($C_9H_{18}N_3$, calcd 168.1495).

5.4. Synthesis of N_α,N_α,N_τ-Trimethyl-histamine ($\mathbf{L}_{\mathbf{Me3}}$). N_τ-Methyl-histamine dihydrochloride was synthesized from histamine-free base through a cyclic urea intermediate.[49] N_α-Dimethylation was adopted from a known procedure.[26] In general, N_τ-methyl-histamine dihydrochloride (1.0 g, 5 mmol), paraformaldehyde (1.5 g, 50 mmol), and sodium cyanoborohydride (3.1 g, 50 mmol) were stirred in 30 mL of 0.2 M N_4HOAc(aq) (pH 5.4) at 40 °C overnight. Solid sodium hydroxide was added until pH ∼13. The aqueous solution was extracted three times with 30 mL of dichloromethane. The organic extracts were combined, dried over granular Na_2SO_4, and concentrated. The crude oil was stirred over crushed CaH_2 overnight before heated distillation under vacuum to give a clear viscous oil. Yield: 0.367 g, 52%. ^{1}H NMR (400 MHz, $CDCl_3$): δ 7.27 (s, 1H, aromatic H), δ 6.60 (s, 1H, aromatic H), δ 3.57 (s, 3H, N_τ-methyl), δ 2.71−2.66 (mult., 2H, 2H, $-CH_2-$), δ 2.58−2.52 (mult., 2H, 2H, $-CH_2-$), δ 2.23 (s, 6H, N_α-methyl). ^{13}C NMR (100.6 MHz, $CDCl_3$): δ 141.30, δ 137.19, δ 116.63, δ 59.63, δ 45.57, δ 33.57, δ 26.90. HRMS (H^+): m/z = 154.1340 ($C_8H_{16}N_3$, calcd 154.1339).

5.5. Synthesis of N_α,N_α-Dimethyl-histamine ($\mathbf{L}_{\mathbf{Me2}}$). Histamine (2.0 g, 18 mmol), paraformaldehyde (2.7 g, 90 mmol), and sodium cyanoborohydride (5.7 g, 90 mmol) were stirred in 60 mL of 0.2 M NH_4OAc(aq) (pH 5.4) at 40 °C overnight. Solid sodium hydroxide was added until pH ∼13. The aqueous solution was extracted four times with 30 mL of dichloromethane. The organic extracts were combined, dried over granular Na_2SO_4, and concentrated. The crude oil was purified by heated distillation under vacuum to give a clear viscous oil. Yield: 0.763 g, 31%. ^{1}H NMR (400 MHz, $CDCl_3$): δ 7.47 (s, 1H, aromatic), δ 6.75 (s, 1H, aromatic H), δ 2.78−2.69 (mult., 2H, $-CH_2-$), δ 2.59−2.52 (mult., 2H, $-CH_2-$), δ 2.27 (s, 6H, N_α-methyl). ^{13}C NMR (100.6 MHz, $CDCl_3$): δ 134.52, δ 134.23, δ 119.23, δ 59.21, δ 45.31, δ 24.11. HRMS (H^+): m/z = 140.1186 ($C_7H_{14}N_3$, calcd 140.1182).

5.6. General Method of Formation of $\mathbf{T}_{\mathbf{nBu}}$ and $\mathbf{T}_{\mathbf{Me3}}$. The optical immersion probe and reaction vessel described above were charged with 5 mL of 2-MeTHF, sealed with a septum, and equilibrated in a $N_2(l)$/acetone frozen slurry (−95 °C). The vessel was purged with 1 atm of O_2 using a fine needle for ca. 10 min to saturate the solution. A 10 mM solution of $[Cu(CH_3CN)_4]SbF_6$ and L ($\mathbf{L}_{\mathbf{nBu}}$, $\mathbf{L}_{\mathbf{Me3}}$) in 500 μL of THF was injected slowly into the solution (1 mM Cu), leading to formation of $\mathbf{T}_{\mathbf{nBu}}$ and $\mathbf{T}_{\mathbf{Me3}}$ after 3 min of stirring.

5.7. General Method of Formation of $\mathbf{T}_{\mathbf{Me2}}$. The optical immersion probe and reaction vessel described above were charged with 5 mL of 2-MeTHF, sealed with a septum, and equilibrated in a $N_2(l)$/acetone frozen slurry (−95 °C). The vessel was purged with 1 atm of O_2 using a fine needle for ca. 10 min to saturate the solution. Next, 250 μL of 20 mM $\mathbf{L}_{\mathbf{Me2}}$ and 250 μL of 20 mM $[Cu(CH_3CN)_4]$-SbF_6 were sequentially injected slowly into the solution (1 mM Cu), leading to formation of $\mathbf{T}_{\mathbf{Me2}}$ after 3 min of stirring.

5.8. O_2 Titration with $\mathbf{L}_{\mathbf{nBu}}$. The optical immersion probe and reaction vessel described above were charged with 5 mL of a 10 mM solution of $[Cu(CH_3CN)_4]SbF_6$ and $\mathbf{L}_{\mathbf{nBu}}$ in 2-MeTHF, sealed with a septum, and equilibrated in a $N_2(l)$/pentane frozen slurry (−125 °C) under an atmosphere of N_2. Next, 500 μL aliquots (0.1 equiv) of O_2-saturated THF (10 mM) were injected and allowed to maximize formation. Each spectrum of the titrated species was allowed to stabilize for at least 2 min before addition of more titrant. Fitting the two linear regions of the absorbance (457 nm, Figure S10) changes versus equivalents allows the Cu/O_2 ratio to be the crossing point of the two linear regions (0.33 equiv of O_2) or Cu/O_2 of 3.0.

5.9. O_2 Titration with $\mathbf{L}_{\mathbf{Me3}}$. The optical immersion probe and reaction vessel described above were charged with 5 mL of a 10 mM solution of $[Cu(CH_3CN)_4]SbF_6$ and $\mathbf{L}_{\mathbf{Me3}}$ in dried 2-MeTHF, sealed with a septum, and equilibrated in a $N_2(l)$/pentane frozen slurry (−125 °C) under an atmosphere of N_2. Next, 500 μL aliquots (0.1 equiv) of O_2-saturated THF (10 mM) were injected and allowed to maximize formation. Each spectrum of the titrated species was allowed to stabilize for at least 2 min before addition of more titrant. Fitting the two linear regions of the absorbance (510 nm, Figure S11) changes versus equivalents allows the Cu/O_2 ratio to be the crossing point of the two linear regions (0.31 equiv of O_2) or Cu/O_2 of 3.2.

5.10. $\mathbf{O}_{\mathbf{Me3}}$ to $\mathbf{T}_{\mathbf{Me3}}$ Conversion. $\mathbf{O}_{\mathbf{Me3}}$ was made according to previously reported methods at 1 mM [Cu] at −125 °C in a $N_2(l)$/pentane frozen slurry.[22] O_2 was removed from the system by purging with N_2 for 10 min. Next, 250 μL (1 equiv to $\mathbf{O}_{\mathbf{Me3}}$) of a 10 mM solution of $[Cu\mathbf{L}_{\mathbf{Me3}}(CH_3CN)_2]SbF_6$ was added, and the reaction was monitored by UV−vis.

5.11. Geometric Predictions for $\mathbf{T}_{\mathbf{Me3}}$ and $\mathbf{T}_{\mathbf{nBu}}$. Geometry optimizations of $\mathbf{T}_{\mathbf{Me3}}$ and $\mathbf{T}_{\mathbf{nBu}}$ (butyl group was modeled as a methyl group, $\mathbf{T}_{\mathbf{Me}}$) were performed in C_1 symmetry at the B3lyp/6-31g(d) level of theory in the gas phase with Gaussian09.[50−52] Optimized calculation structures are tabulated in the Supporting Information. Of the multiple *cis/trans* isomers tested, the lowest energy structure has a *trans* relationship of the histamine ligands on the two Cu(II) metal centers.

5.12. High-Resolution Mass Spectrometry of $\mathbf{T}_{\mathbf{nBu}}$ and $\mathbf{T}_{\mathbf{Me3}}$. $\mathbf{T}_{\mathbf{nBu}}$ and $\mathbf{T}_{\mathbf{Me3}}$ were formed as described above and stored at −125 °C in a $N_2(l)$/pentane frozen slurry prior to analysis. The solution was injected quickly by syringe into the mass spectrometer. No special care was undertaken to control syringe temperature. The resulting **T** clusters were observed as monocations with two associated SbF_6 anions (Figures S12−S15).

5.13. Titrations of $\mathbf{T}_{\mathbf{nBu}}$, $\mathbf{T}_{\mathbf{Me3}}$, and $\mathbf{T}_{\mathbf{Me2}}$ with Decamethylferrocene. $\mathbf{T}_{\mathbf{nBu}}$, $\mathbf{T}_{\mathbf{Me3}}$, and $\mathbf{T}_{\mathbf{Me2}}$ were formed by the method described above. Assuming a concentration [Cu] = 1 mM, 1/10 equiv of decamethylferrocene ($1e^-$ reductant) in THF was added to deoxygenated solutions of $\mathbf{T}_{\mathbf{nBu}}$, $\mathbf{T}_{\mathbf{Me3}}$, and $\mathbf{T}_{\mathbf{Me2}}$ as formed above at −95 °C. Each spectrum of the titrated species was allowed to stabilize for at least 2 min before addition of more titrant. The resulting titration spectra and absorbance versus equivalent plots are shown in the Supporting Information. Titration data were used to established typical formation yields of complexes $\mathbf{T}_{\mathbf{nBu}}$, $\mathbf{T}_{\mathbf{Me3}}$, and $\mathbf{T}_{\mathbf{Me2}}$. Optical data for one UV band and one visible band are illustrated (Figures S1−S9) with good agreement between the two wavelengths for each complex. Lower bound estimates of formation yields are 70%, 80%, and 40% of complexes $\mathbf{T}_{\mathbf{nBu}}$, $\mathbf{T}_{\mathbf{Me3}}$, and $\mathbf{T}_{\mathbf{Me2}}$, respectively.

5.14. Mixture of $\mathbf{T}_{\mathbf{nBu}}$ and $\mathbf{O}_{\mathbf{nBu}}$. The optical immersion probe and reaction vessel described above were charged with 5 mL of 2-MeTHF, sealed with a septum, and equilibrated in a $N_2(l)$/pentane frozen slurry (−125 °C). The vessel was purged with 1 atm of O_2 using a fine needle for ca. 10 min to saturate the solution. A 10 mM solution of $[Cu(CH_3CN)_4]SbF_6$ and $\mathbf{L}_{\mathbf{nBu}}$ in 500 μL of THF was injected slowly into the solution, leading to formation of a mixture of $\mathbf{T}_{\mathbf{nBu}}$ and $\mathbf{O}_{\mathbf{nBu}}$

DOI: 10.1021/jacs.6b05538
J. Am. Chem. Soc. 2016, 138, 9986−9995

after 5 min of stirring. The mixture was fit by addition of pure optical spectra for independently synthesized $\mathbf{T}_{\mathbf{nBu}}$ and $\mathbf{O}_{\mathbf{nBu}}$ (Figure S16).

5.15. Mixture of $\mathbf{T}_{\mathbf{Me3}}$ and $\mathbf{O}_{\mathbf{Me3}}$. The optical immersion probe and reaction vessel described above were charged with 11 mL of purified and distilled 2-MeTHF, sealed with a septum, and equilibrated in a $N_2(l)$/pentane frozen slurry (~ −125 °C). The vessel was purged with pure O_2 using a fine needle for ca. 10 min to saturate the solution. A 10 mM solution of $[Cu(CH_3CN)_4]SbF_6$ and $\mathbf{L}_{\mathbf{Me3}}$ in 110 μL of THF was injected slowly into the solution, leading to formation of a mixture of $\mathbf{T}_{\mathbf{Me3}}$ and $\mathbf{O}_{\mathbf{Me3}}$ after 5 min of stirring. The mixture wass fit by addition of pure optical spectra for independently synthesized $\mathbf{T}_{\mathbf{Me3}}$ and $\mathbf{O}_{\mathbf{Me3}}$ (Figure S17).

5.16. Reactions of O and T with Ascorbic Acid. $\mathbf{O}_{\mathbf{nBu}}$ and $\mathbf{O}_{\mathbf{Me3}}$ were prepared by core capture strategies.[22] $\mathbf{T}_{\mathbf{nBu}}$ and $\mathbf{T}_{\mathbf{Me3}}$ were prepared as illustrated above at −125 °C in a $N_2(l)$/pentane frozen slurry. 5,6-Isopropylidene-L-ascorbic acid was added, and the decomposition was monitored by UV−vis. Kinetic rates are detailed in the Supporting Information (Table S1).

5.17. Computational Isodesmic Reaction Energies. Geometry optimizations were performed in C_1 or C_i symmetry (when possible) at the M06/TZVP level of theory using an SMD (water) solvation model with Gaussian09 at multiple spin states if possible; only lowest energy structure is tabulated in the Supporting Information.[33−36] Single-point structures were calculated at the M06/TZVP level of theory using an SMD (water) solvation model and a second-order relativistic correction (DKH2) with Gaussian09.[37] Optimized structures of all calculated complexes are tabulated in the Supporting Information.

5.18. Marcus Theory Calculations for $\mathbf{T}_{\mathbf{Me3}}$, $\mathbf{T}_{\mathbf{nBu}}$, $\mathbf{O}_{\mathbf{Me3}}$, and $\mathbf{O}_{\mathbf{nBu}}$. Geometry optimizations of $\mathbf{T}_{\mathbf{Me3}}$ and $\mathbf{T}_{\mathbf{nBu}}$ (butyl group was modeled as a methyl group $\mathbf{T}_{\mathbf{Me}}$) were performed in C_1 symmetry at the M06/TZVP level of theory using an SMD (water) solvation model with Gaussian 09 with multiple spin states if possible; only lowest energy structure is tabulated in the Supporting Information.[33−36] Single-point structures were calculated at the M06/TZVP level of theory using an SMD (water) solvation model and a second-order relativistic correction (DKH2) with Gaussian 09.[37] Associated $\mathbf{O}_{\mathbf{Me3}}$ and $\mathbf{O}_{\mathbf{nBu}}$ (butyl group was modeled as a methyl group $\mathbf{O}_{\mathbf{Me}}$) structures were calculated in either C_1 or C_i symmetry when viable. H-atoms were placed at geometrically equivalent positions in the oxidized forms as found in the optimized structures of the reduced form. Optimized structures of all calculated complexes are tabulated in the Supporting Information.

■ ASSOCIATED CONTENT

Supporting Information

The Supporting Information is available free of charge on the ACS Publications website at DOI: 10.1021/jacs.6b05538.

Experimental procedures, results, computational details, and spectroscopic data (PDF)

■ AUTHOR INFORMATION

Corresponding Author

*stack@stanford.edu

Notes

The authors declare no competing financial interest.

■ ACKNOWLEDGMENTS

J.B.G. acknowledges the NIH Ruth L. Kirschstein National Research Service Fellowship 5F32GM103071 for financial support. T.A.B. thanks the Center for Molecular Analysis and Design (CMAD) for a graduate fellowship. Use of the Stanford Synchrotron Radiation Lightsource, SLAC National Accelerator Laboratory, is supported by the U.S. Department of Energy, Office of Science, Office of Basic Energy Sciences under Contract No. DE-AC02-76SF00515. The SSRL Structural Molecular Biology Program is supported by the DOE Office of Biological and Environmental Research, and by the National Institutes of Health, National Institute of General Medical Sciences (including P41GM103393). The contents of this publication are solely the responsibility of the authors and do not necessarily represent the official views of NIGMS or NIH. This work was supported by a subcontract with the University of Utah (Agreement 10029173-S2) for which the Air Force Office of Scientific Research (Grant FA9550-12-1-0481) is the prime sponsor.

■ REFERENCES

(1) Solomon, E. I.; Heppner, D. E.; Johnston, E. M.; Ginsbach, J. W.; Cirera, J.; Qayyum, M.; Kieber-Emmons, M. T.; Kjaergaard, C. H.; Hadt, R. G.; Tian, L. *Chem. Rev.* **2014**, *114*, 3659−3853.

(2) Lewis, E. A.; Tolman, W. B. *Chem. Rev.* **2004**, *104*, 1047−1076.

(3) Mirica, L. M.; Ottenwaelder, X.; Stack, T. D. P. *Chem. Rev.* **2004**, *104*, 1013−1045.

(4) Citek, C.; Lyons, C. T.; Wasinger, E. C.; Stack, T. D. P. *Nat. Chem.* **2012**, *4*, 317−322.

(5) Lee, Y.; Park, G. Y.; Lucas, H. R.; Vajda, P. L.; Kamaraj, K.; Vance, M. A.; Milligan, A. E.; Woertink, J. S.; Siegler, M. A.; Narducci Sarjeant, A. A.; Zakharov, L. N.; Rheingold, A. L.; Solomon, E. I.; Karlin, K. D. *Inorg. Chem.* **2009**, *48*, 11297−11309.

(6) Sorrell, T. N.; Allen, W. E.; White, P. S. *Inorg. Chem.* **1995**, *34*, 952−960.

(7) Lynch, W. E.; Kurtz, D. M.; Wang, S. K.; Scott, R. A. *J. Am. Chem. Soc.* **1994**, *116*, 11030−11038.

(8) Sanyal, I.; Karlin, K. D.; Strange, R. W.; Blackburn, N. J. *J. Am. Chem. Soc.* **1993**, *115*, 11259−11270.

(9) Sanyal, I.; Strange, R. W.; Blackburn, N. J.; Karlin, K. D. *J. Am. Chem. Soc.* **1991**, *113*, 4692−4693.

(10) Quinlan, R. J.; Sweeney, M. D.; Lo Leggio, L.; Otten, H.; Poulsen, J.-C. N.; Johansen, K. S.; Krogh, K. B. R. M.; Jørgensen, C. I.; Tovborg, M.; Anthonsen, A.; Tryfona, T.; Walter, C. P.; Dupree, P.; Xu, F.; Davies, G. J.; Walton, P. H. *Proc. Natl. Acad. Sci. U. S. A.* **2011**, *108*, 15079−15084.

(11) Kjaergaard, C. H.; Qayyum, M. F.; Wong, S. D.; Xu, F.; Hemsworth, G. R.; Walton, D. J.; Young, N. A.; Davies, G. J.; Walton, P. H.; Johansen, K. S.; Hodgson, K. O.; Hedman, B.; Solomon, E. I. *Proc. Natl. Acad. Sci. U. S. A.* **2014**, *111*, 8797−8802.

(12) Lieberman, R. L.; Shrestha, D. B.; Doan, P. E.; Hoffman, B. M.; Stemmler, T. L.; Rosenzweig, A. C. *Proc. Natl. Acad. Sci. U. S. A.* **2003**, *100*, 3820−3825.

(13) Balasubramanian, R.; Smith, S. M.; Rawat, S.; Yatsunyk, L. A.; Stemmler, T. L.; Rosenzweig, A. C. *Nature* **2010**, *465*, 115−U131.

(14) Himes, R. A.; Barnese, K.; Karlin, K. D. *Angew. Chem., Int. Ed.* **2010**, *49*, 6714−6716.

(15) Lawton, T. J.; Ham, J.; Sun, T.; Rosenzweig, A. C. *Proteins: Struct., Funct., Genet.* **2014**, *82*, 2263−2267.

(16) Liew, E. F.; Tong, D.; Coleman, N. V.; Holmes, A. J. *Microbiology* **2014**, *160*, 1267−1277.

(17) Hatzenpichler, R. *Appl. Environ. Microbiol.* **2012**, *78*, 7501−7510.

(18) Jin, T.; Zhang, T.; Yan, Q. *Appl. Microbiol. Biotechnol.* **2010**, *87*, 1167−1176.

(19) Rotthauwe, J. H.; Witzel, K. P.; Liesack, W. *Appl. Environ. Microbiol.* **1997**, *63*, 4704−4712.

(20) Schatz, M.; Leibold, M.; Foxon, S. P.; Weitzer, M.; Heinemann, F. W.; Hampel, F.; Walter, O.; Schindler, S. *Dalton Trans.* **2003**, 1480−1487.

(21) Schindler, S. *Eur. J. Inorg. Chem.* **2000**, *2000*, 2311−2326.

(22) Citek, C.; Gary, J. B.; Wasinger, E. C.; Stack, T. D. P. *J. Am. Chem. Soc.* **2015**, *137*, 6991−6994.

(23) Citek, C.; Lin, B.-L.; Phelps, T. E.; Wasinger, E. C.; Stack, T. D. P. *J. Am. Chem. Soc.* **2014**, *136*, 14405−14408.

(24) *Oxygen and Ozone*; Pergamon: Elmsford, NY, 1981; pp 261−305.

DOI: 10.1021/jacs.6b05538
J. Am. Chem. Soc. 2016, 138, 9986−9995

(25) Cole, A. P.; Root, D. E.; Mukherjee, P.; Solomon, E. I.; Stack, T. D. P. *Science* **1996**, *273*, 1848−1850.
(26) Taki, M.; Teramae, S.; Nagatomo, S.; Tachi, Y.; Kitagawa, T.; Itoh, S.; Fukuzumi, S. *J. Am. Chem. Soc.* **2002**, *124*, 6367−6377.
(27) Kang, P.; Bobyr, E.; Dustman, J.; Hodgson, K. O.; Hedman, B.; Solomon, E. I.; Stack, T. D. P. *Inorg. Chem.* **2010**, *49*, 11030−11038.
(28) Gupta, A. K.; Tolman, W. B. *Inorg. Chem.* **2012**, *51*, 1881−1888.
(29) Lionetti, D.; Day, M. W.; Agapie, T. *Chem. Sci.* **2013**, *4*, 785−790.
(30) Kau, L. S.; Spira-Solomon, D. J.; Penner-Hahn, J. E.; Hodgson, K. O.; Solomon, E. I. *J. Am. Chem. Soc.* **1987**, *109*, 6433−6442.
(31) DuBois, J. L.; Mukherjee, P.; Collier, A. M.; Mayer, J. M.; Solomon, E. I.; Hedman, B.; Stack, T. D. P.; Hodgson, K. O. *J. Am. Chem. Soc.* **1997**, *119*, 8578−8579.
(32) Mixing and diffusion at these extreme low temperatures limit the rate at which kinetic measurements are possible, and $\mathbf{O}_{\mathbf{Me3}}/\mathbf{O}_{\mathbf{nBu}}$ react as fast as can be measured with our current experimental setup.
(33) Zhao, Y.; Truhlar, D. *Theor. Chem. Acc.* **2008**, *120*, 215−241.
(34) Schäfer, A.; Horn, H.; Ahlrichs, R. *J. Chem. Phys.* **1992**, *97*, 2571−2577.
(35) Schäfer, A.; Huber, C.; Ahlrichs, R. *J. Chem. Phys.* **1994**, *100*, 5829−5835.
(36) Marenich, A. V.; Cramer, C. J.; Truhlar, D. G. *J. Phys. Chem. B* **2009**, *113*, 6378−6396.
(37) Barysz, M.; Sadlej, A. J. *J. Mol. Struct.: THEOCHEM* **2001**, *573*, 181−200.
(38) Root, D. E.; Henson, M. J.; Machonkin, T.; Mukherjee, P.; Stack, T. D. P.; Solomon, E. I. *J. Am. Chem. Soc.* **1998**, *120*, 4982−4990.
(39) Daul, C. A.; Fernandez-Ceballos, S.; Ciofini, I.; Rauzy, C.; Schläpfer, C.-W. *Chem. - Eur. J.* **2002**, *8*, 4392−4401.
(40) Bérces, A. *Chem. - Eur. J.* **1998**, *4*, 1297−1304.
(41) Mayer, J. M. *J. Phys. Chem. Lett.* **2011**, *2*, 1481−1489.
(42) Kaim, W.; Rall, J. *Angew. Chem., Int. Ed. Engl.* **1996**, *35*, 43−60.
(43) Crichton, R. R.; Pierre, J. L. *BioMetals* **2001**, *14*, 99−112.
(44) Stack, T. D. P. *Dalton Trans.* **2003**, *10*, 1881−1889.
(45) Mahadevan, V.; Henson, M. J.; Solomon, E. I.; Stack, T. D. P. *J. Am. Chem. Soc.* **2000**, *122*, 10249−10250.
(46) Ottenwaelder, X.; Rudd, D. J.; Corbett, M. C.; Hodgson, K. O.; Hedman, B.; Stack, T. D. P. *J. Am. Chem. Soc.* **2006**, *128*, 9268−9269.
(47) Cahoy, J.; Holland, P. L.; Tolman, W. B. *Inorg. Chem.* **1999**, *38*, 2161−2168.
(48) Kubas, G. J.; Monzyk, B.; Crumbliss, A. L. *Inorg. Synth.* **1979**, *19*, 90−92.
(49) Saulnier, M. G.; Frennesson, D. B.; Wittman, M. D.; Zimmermann, K.; Velaparthi, U.; Langley, D. R.; Struzynski, C.; Sang, X.; Carboni, J.; Li, A.; Greer, A.; Yang, Z.; Balimane, P.; Gottardis, M.; Attar, R.; Vyas, D. *Bioorg. Med. Chem. Lett.* **2008**, *18*, 1702−1707.
(50) Becke, A. D. *J. Chem. Phys.* **1993**, *98*, 5648−5652.
(51) Petersson, G. A.; Bennett, A.; Tensfeldt, T. G.; Al-Laham, M. A.; Shirley, W. A.; Mantzaris, J. *J. Chem. Phys.* **1988**, *89*, 2193−2218.
(52) Petersson, G. A.; Al-Laham, M. A. *J. Chem. Phys.* **1991**, *94*, 6081−6090.

DOI: 10.1021/jacs.6b05538
J. Am. Chem. Soc. 2016, 138, 9986−9995